Precision Engineering 34 (2010) 659–666

Contents lists available at ScienceDirect

Precision Engineering

journal homepage: www.elsevier.com/locate/precision

Technical note

Dimensionless design graphs for three types of annulus-shaped flexure hinges

Bi Shusheng [a,*], Zhao Shanshan [a], Zhu Xiaofeng [b]

[a] A-316, Robotics Institute, Beihang University, Beijing, 100191, PR China
[b] Beijing Municipal Institute of Labor Protection, Beijing, 100054, PR China

ARTICLE INFO

Article history:
Received 3 February 2009
Received in revised form 1 December 2009
Accepted 4 January 2010
Available online 13 January 2010

Keywords:
Annulus-shaped flexure hinge
Dimensionless design graph
Preliminary design

ABSTRACT

An annulus-shaped flexure hinge is composed of three or more beam flexure elements distributed in an annulus suitable for rotational application, such as laser tracking system and cell operation system. The load-deflection property of annulus-shaped flexure hinges can be analyzed by traditional beam deformation expressions or pseudo-rigid-body method accurately and effectively, but methods are incapable to choose the type of hinge and the key parameters in a quick and exact way. In order to avoid laborious design steps, dimensionless design graphs for a novel annulus-shaped flexure hinge and another two types are presented which are based on finite element analysis. Using these graphs as a design tool, designers can determine the optimal geometry, based on the stiffness and demanded rotational properties of annulus-shaped flexure hinge. Between the analyzed flexure hinges, a comparison is made on the basis of equal hinge functionality: rotational properties for different hinges. The result describes the maximum stiffness properties from different hinges in identical situations. The straight-compliant annulus-shaped flexure hinge is preferred for radius stiffness and rotation stiffness. The curved-compliant annulus-shaped flexure hinge has the best axial stiffness. The instances of using dimensionless design graph are given and results indicate that the relative error between dimensionless graph and design demand is below 4%. Using the dimensionless design graph, design process can be reduced in both time and complexity.

1. Introduction

Flexure hinges are increasingly popular with designs requiring one-piece (monolithic) manufacturing, reduced weight, motion smoothness, and virtually infinite resolution, zero backlash, friction, and lubrication. Due to this advantages flexure hinges are commonly used in precision engineering [1–3], metrology [4] and aerospace fields [5] for example.

Flexure elements of annulus-shaped flexure hinge are well-proportioned distributed in the closed-loop annulus structure. On the assumption that the material of flexure hinge is linear, elastic and isotropic, structural characteristic of annulus-shapes make sure that there is theoretically no excursion of rotational center with the pure torque. Straight beam flexure elements (SBFEs) and lump-straight beam flexure elements (LSBFEs) appear commonly in existing annulus-shaped flexure hinges [6,7], but curved beam flexure elements (CBFEs) are rarely found. Here we present a new configuration that can be constructed by arraying CBFEs symmetrically in an annulus.

Because there are several flexure elements in an annulus, the structure is complex and difficult to analyze capacity.

Existing methods [8–14] can analyze performance exactly and effectively, but designers cannot choose the type of annulus-shaped flexure hinge and confirm key structural parameters in a fast way.

In this paper, dimensionless design graphs of three types of annulus-shaped flexure hinges are established by a structure-interrelated dimensionless factor. Finite element calculations which can be assumed to be the 'truth' [15] are used to construct dimensionless design graphs. The relationship between geometry and hinge behavior are presented both numerically and graphically, to assist designers constructively in the process of choosing both the type of flexure hinge and the geometry during the first stages of the design process.

2. Annulus-shaped flexure hinge

2.1. Deformation properties of flexure elements

The beam flexure is a classical element for flexure hinges and can be differentiated into three species: SBFE, LSBFE (the lump is in the center of SBFE) and CBFE. While one end is fixed and another end connected to the load, there are different deformation properties.

A SBFE with vector force F at the free end (point A) is shown in Fig. 1(a). The point O is the fixed end. L denotes the length of OA which is the initial length. For the deformation of SBFE, the point A moves to the point A1. B1 denotes the length of OA1. Suppos-

* Corresponding author.
E-mail address: biss_buaa@163.com (B. Shusheng).

0141-6359/$ – see front matter © 2010 Elsevier Inc. All rights reserved.
doi:10.1016/j.precisioneng.2010.01.002

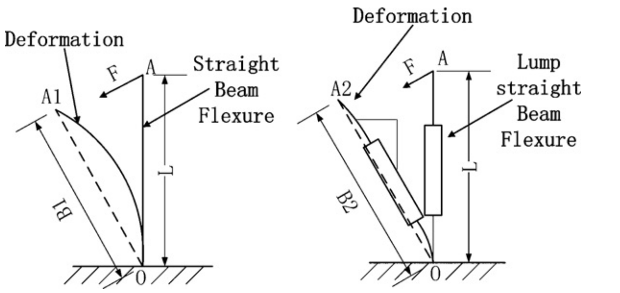

Fig. 1. Deformation of SBFE and LSBFE. (a) Deformation of SBFE and (b) deformation of LSBFE.

ing the beam length is constant, the deformation of SBFE results in decreasing the distance between fixed end point and free end point

$$B1 < L \tag{1}$$

SBFE only deforms to decrease the distance between the free and fixed end point that property is defined as single directional deformation property or negative deformation property.

A LSBFE where a vector force F acts at the free end (point A) is shown in Fig. 1(b). The point O is the fixed end. L denotes the length of OA which is the initial length. For the deformation of LSBFE, the point A moves to the point A2. B2 denotes the length of OA2. Supposing the beam length is constant, the deformation of LSBFE results in decreasing the distance between fixed end point and free end point

$$B2 < L \tag{2}$$

LSBFE only deforms to decrease the distance of line which joins fixed end point and free end point that is defined as single directional deformation property or negative deformation property.

The CBFE deflection characteristic is different from the SBFE or LSBFE. A CBFE where a vector force F acts at the free end (point A) is shown in Fig. 2. The point O is the fixed end. L denotes the length of OA which is initial length.

With a vector force at the free end which is shown in Fig. 2(a), the point A moves to the point A3. B3 denotes the length of OA3.

$$B3 < L \tag{3}$$

The CBFE deforms to decrease the distance of line which joins fixed end point and free end point that can be defined as negative deformation property.

With the force at the free end which is shown in Fig. 2(b), the point A moves to the point A4. B4 denotes the length of OA4.

$$B4 > L \tag{4}$$

The CBFE deforms to increase the distance of line which joins fixed end point and free end point that can be defined as positive deformation property.

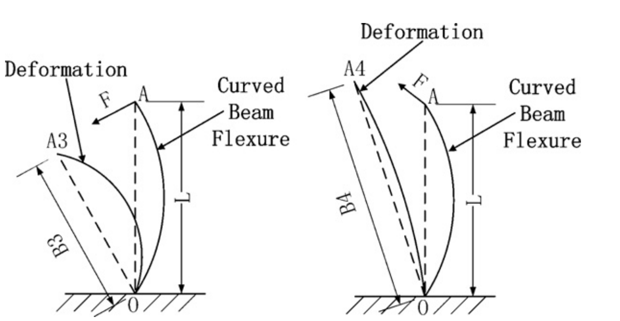

Fig. 2. Deformation of CBFE. (a) CBFE under negative deformation and (b) CBFE under positive deformation.

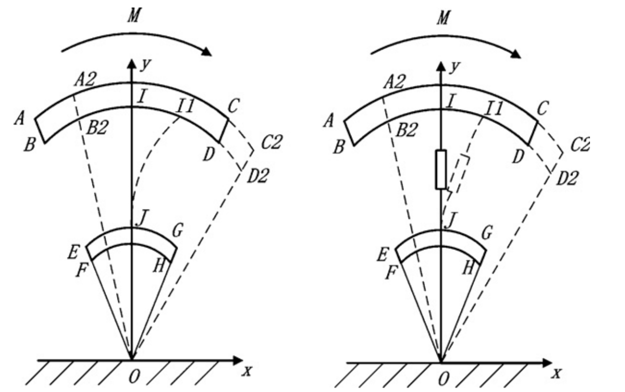

Fig. 3. Flexure module. (a) Straight flexure module and (b) lump-straight flexure module.

The deformation of CBFE can increase or decrease the distance between fixed and free end point so that CBFE has a bidirectional deformation property, a negative deformation property and a positive deformation property.

2.2. Rotational flexure module

The flexure elements mentioned above are suitable for the construction of rotational modules. The rule of construction is that the torsion is equal with the module rotates clockwise and anticlockwise and the number of flexure elements used is minimized. On the basis of the rule of construction, straight flexure module uses one straight flexure element, lump-straight flexure module uses one lump-straight flexure element and curved isosceles-trapezoidal flexure module uses two curved flexure elements for example.

The schematic drawing of a straight flexure module and a lump-straight flexure module is shown in Fig. 3(a) and (b), respectively. The point O is the center of the arc ABCD and EFGH that is fixed. Let arc ABCD rotates clockwise to the position A2B2C2D2 along the path of the arc AC. The flexure element IJ deforms and moves to I1J.

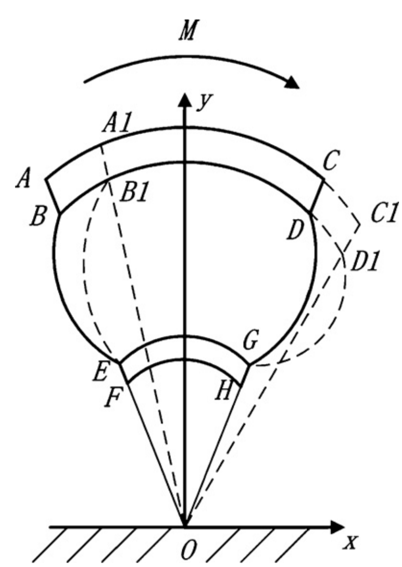

Fig. 4. Curved isosceles-trapezoidal flexure module.

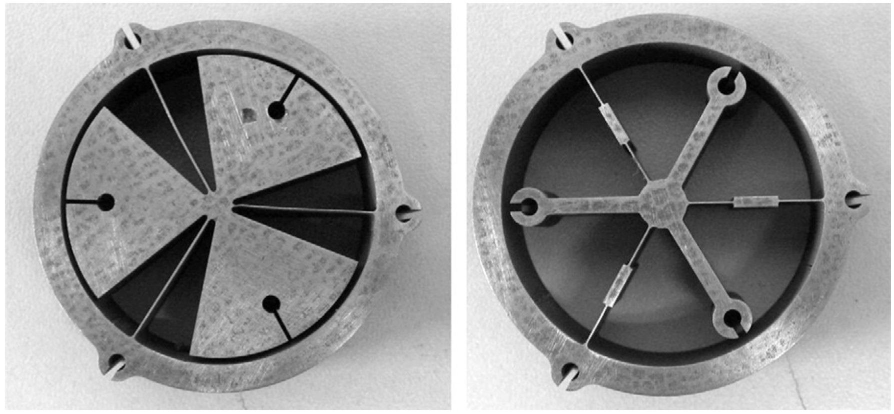

Fig. 5. SCASFH and LCASFH. (a) Straight-compliant annulus-shaped flexure hinge (SCASFH) and (b) lump-compliant annulus-shaped flexure hinge (LCASFH).

Similar to the flexure module mentioned above, the schematic drawing illustrates the curved isosceles-trapezoidal flexure module in Fig. 4. There are two CBFEs in the module based on the rule of construction. The BE and DG make a positive deformation and move to B1E and D1G, respectively. The deformation property of CBFE ensures that the block ABCD rotates a finite angle around the point O.

As pointed out in Ref. [16], an isosceles-trapezoidal flexure hinge has an instantaneous virtual remote center of motion if the angular rotation is small enough, but a curved isosceles-trapezoidal flexure module, which is also a flexure remote center of motion (RCM) mechanism, has the advantage of a fixed virtual center while rotating a finite angle.

2.3. Three types of annulus-shaped flexure hinges

Considering the rational arrangement between mechanical input and output interface, two types of annulus-shaped flexure hinges are obtained using three straight flexure modules and three lump-straight flexure modules as shown in Fig. 5(a) and (b).

Similarly, a novel flexure hinge configuration is constructed by arranging curved isosceles-trapezoidal flexures symmetrically in a circle which is shown in Fig. 6.

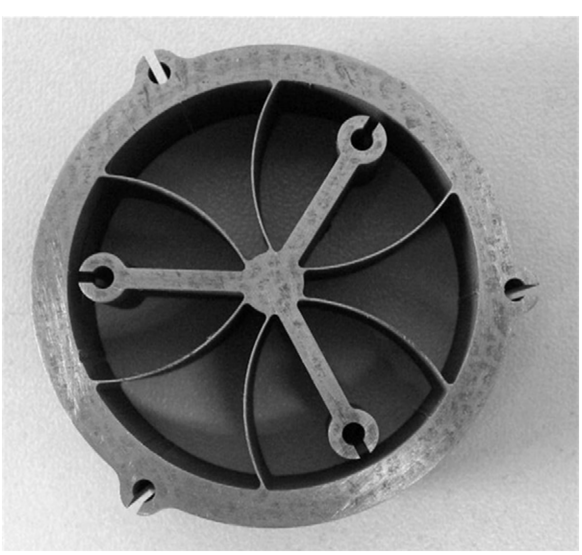

Fig. 6. Curved-compliant annulus-shaped flexure hinge (CCASFH). Relevant coordinate system parameters.

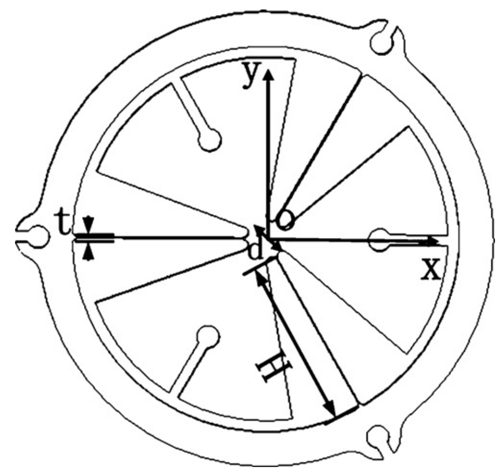

Fig. 7. Relevant coordinate system and parameters of SCASFH.

While, functionally, only three flexure modules in the annulus-shaped flexure hinge are needed to adequately support the rotation, four or more modules may be used as well.

3. Relevant coordinate system parameters

Important design properties for any type of annulus-shaped flexure hinges are stiffness in rotation direction (encircle the point O), stiffness in radial-direction (x-direction or y-direction) and axial-direction (vertical x–y plane) and the stress builds up due to bending (elastic deformation) over an angle. Relevant coordinate system and parameters of SCASFH, LCASFH and CCASFH are shown in Figs. 7–9. The nomenclature used later on is shown in Table 1.

Table 1
Abbreviation and nomenclature of the used parameters.

Nomenclature	
B	Length of lump
c	Stiffness
d	Diameter of inner circle
E	Young's modulus
H	Length of SBFE
h	Thickness of flexure hinge
k	Rotation stiffness
L	Length of LSBFE
P	Chord length of CBFE
R	Radius of CBFE
t	Thickness of flexure element
x, y	Reference axes
σ	Stress

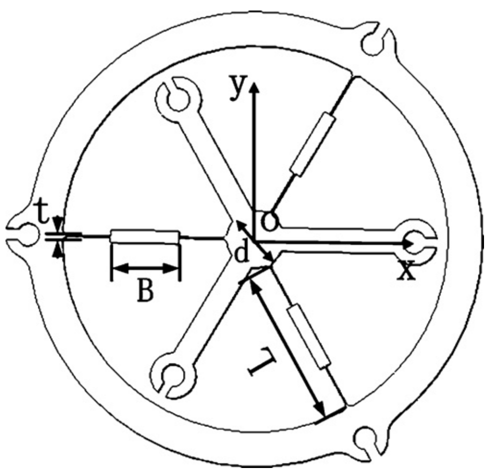

Fig. 8. Relevant coordinate system and parameters of LCASFH.

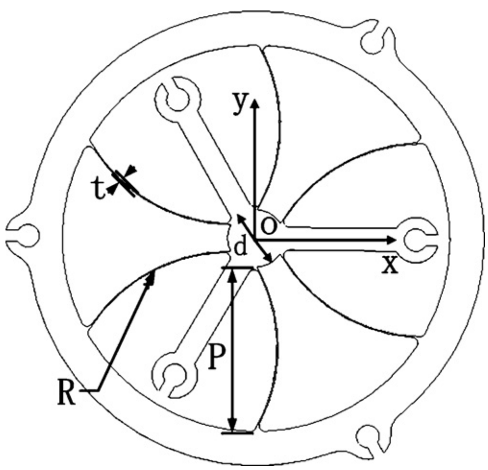

Fig. 9. Relevant coordinate system and parameters of CCASFH.

4. Dimensionless design equations and graphs

Dimensionless design equations and graphs are given using structure-interrelated dimensionless factor. In order to calculate the rotation stiffness expediently, the diameter of inner circle of SCASFH, LCASFH and CCASFH are settled on 4 mm for the numerical analysis.

The dimensionless design graph for SCASFH is produced using the finite element calculations program ANSYS. The most important aspects of the finite element programming can be summarized:

Table 2
Fit errors of SCASFH.

SCASFH	Adjusted R-square
Radial-direction	0.9946
Axial-direction	0.9915
Rotational stiffness	0.9388
Rotational stress	0.9869

- ANSYS version 11.0.
- Element type: SOLID95.
- Material properties: the Young's modulus used in that of titanium alloy: 95 GPa. The Poisson's ratio used is 0.41.

4.1. SCASFH

The performance of annulus-shaped flexure hinge is determined by the flexure element so that structure parameters for flexure element are the key parameters of annulus-shaped flexure hinge. The key parameters of SCASFH are thickness (t) and length (H) of SBFE. The dimensionless structure-interrelated factor is defined as the ratio of thickness (t) and length (H) of SBFE:

$$\varsigma = \sqrt{\frac{t}{H}} \tag{5}$$

The use of the square root is merely to enlarge the clarity of the graph for smaller ratios, which are most realistic for practical use. In order to characterize the annulus-shaped flexure hinge more mathematically, the large number of data points (12 per graph line) are fitted with a function. In this case, the equations of the curves are formed by third order polynomial fitting.

For a SCASFH, equations for the dimensionless numbers are given below. The fit errors are shown in Table 2.

Dimensionless stiffness radial-direction C_{radial}:

$$\frac{C_{\mathrm{radial}}}{E \times h} = 13.9941\varsigma^3 - 4.6133\varsigma^2 + 0.9014\varsigma - 0.0414 \tag{6}$$

Dimensionless stiffness in axial-direction C_{axial}:

$$\frac{C_{\mathrm{axial}}}{E \times h} = 2.8361\varsigma^3 - 0.9683\varsigma^2 + 0.3415\varsigma - 0.0204 \tag{7}$$

Dimensionless rotation stiffness k:

$$\frac{12 \times k}{E \times h \times t^2} = 86.7667\varsigma^3 - 38.1744\varsigma^2 + 5.5177\varsigma - 0.2325 \tag{8}$$

Dimensionless rotation stress σ:

$$\frac{\sigma}{\varphi \times E} = 1.2175\varsigma^3 - 0.4496\varsigma^2 + 0.066\varsigma - 0.0021 \tag{9}$$

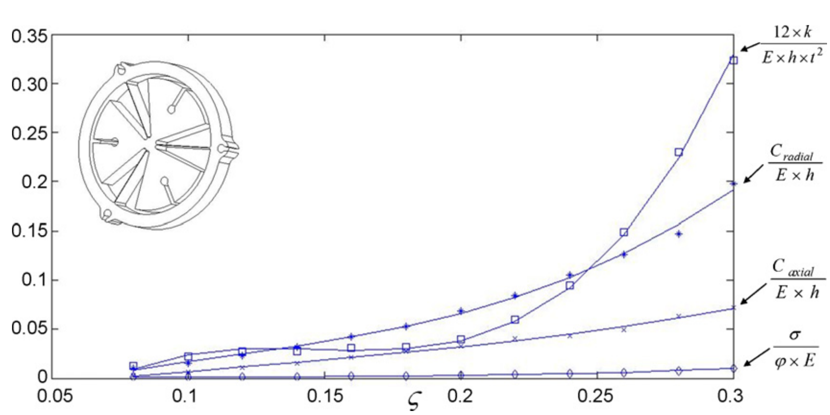

Fig. 10. Dimensionless design graph for SCASFH.

Table 3
Fit errors of LCASFH.

LCASFH	Adjusted R-square
Radial-direction	0.9862
Axial-direction	0.9958
Rotational stiffness	0.9709
Rotational stress	0.9847

Table 4
Fit errors of CCASFH.

CCASFH	Adjusted R-square
Radial-direction	0.9997
Axial-direction	0.9987
Rotational stiffness	0.9995
Rotational stress	0.9819

The equations describe the stiffness for a SCASFH directly as a function of the geometry, as represented graphically in Fig. 10.

4.2. LCASFH

The key parameters of LCASFH are thickness (t), length (L) and length of lump (B) of LSBFE. The dimensionless structure-interrelated factor is the ratio of curved flexure element thickness (t) and the value of length (L) minus length of (B):

$$\zeta = \sqrt{\frac{t}{L - B}} \tag{10}$$

For LCASFH equations, the dimensionless numbers are given below. The fit errors are shown in Table 3.

Dimensionless stiffness in radial-direction C_{radial}:

$$\frac{C_{\text{radial}}}{E \times h} = -0.03627\zeta^3 - 0.3813\zeta^2 + 0.5673\zeta - 0.0442 \tag{11}$$

Dimensionless stiffness in axial-direction C_{axial}:

$$\frac{C_{\text{axial}}}{E \times h} = 0.4403\zeta^3 - 0.3224\zeta^2 + 0.1359\zeta - 0.0067 \tag{12}$$

Dimensionless rotation stiffness k:

$$\frac{12 \times k}{E \times h \times t^2} = -4.0647\zeta^3 + 2.4047\zeta^2 - 0.3805\zeta + 0.0379 \tag{13}$$

Dimensionless rotation stress σ:

$$\frac{\sigma}{\varphi \times E} = 1.6945\zeta^3 - 0.7156\zeta^2 + 0.1101\zeta - 0.0042 \tag{14}$$

The equations describe the stiffness for LCASFH directly as a function of the geometry, as represented graphically in Fig. 11.

4.3. CCASFH

The key parameters of CCASFH are thickness (t), radius (R) and chord length (P) of CBFE. The dimensionless structure-interrelated factor is the ratio of thickness (t) and arc length (L):

$$\xi = \sqrt{\frac{t}{L}} \tag{15}$$

where L is

$$L = \frac{\pi P \sin^{-1}(P/2R)}{90} \tag{16}$$

For CCASFH equations, the dimensionless numbers are given below. The fit errors are shown in Table 4.

Dimensionless stiffness in radial-direction C_{radial}:

$$\frac{C_{\text{radial}}}{E \times h} = 1.4241\xi^3 - 0.2433\xi^2 + 0.0117\xi - 0.0001 \tag{17}$$

where h is thickness of annulus-shaped flexure hinge.

Dimensionless stiffness in axial-direction C_{axial}:

$$\frac{C_{\text{axial}}}{E \times h} = -1.7773\xi^3 + 1.0115\xi^2 - 0.0872\xi + 0.0019 \tag{18}$$

Dimensionless rotation stiffness k:

$$\frac{12 \times k}{E \times h \times t^2} = -0.882\xi^3 + 0.4737\xi^2 + 0.0323\xi + 0.0008 \tag{19}$$

Dimensionless rotation stress σ:

$$\frac{\sigma}{\varphi \times E} = -0.0148\xi^3 + 0.0021\xi^2 + 0.0066\xi - 0.0001 \tag{20}$$

The equations describe the stiffness for a CCASFH directly as a function of the geometry, as represented graphically in Fig. 12.

5. Comparison

Now that the three annulus-shaped flexure hinges are analyzed, it is possible to make a comparison and determine the most favorable. The hinges are compared on the basis of function: an equal rotation angle. The question to answer is: which type has the highest possible stiffness in radial and axial-direction, at equivalent stress levels.

The dimensionless equations and graphs indicate the deflection of rotation, hereby the diameter of inner circle of flexure hinge influences rotational stroke significant. For a feasible comparing the diameter of inner circle of SCASFH, LCASFH and CCASFH are all 4 mm.

For SCASFH, LCASFH and CCASFH, dimensionless design graphs are constructed which relate the stress, stiffness and rotation properties directly to the geometry. Based on the design graphs, a

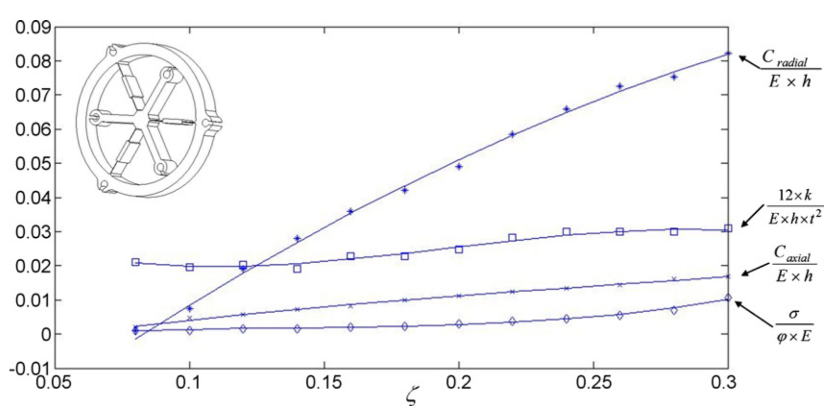

Fig. 11. Dimensionless design graph for LCASFH.

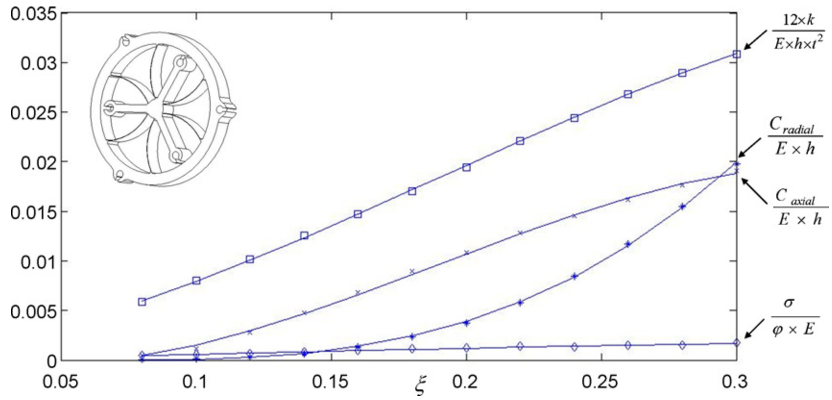

Fig. 12. Dimensionless design graph for CCASFH.

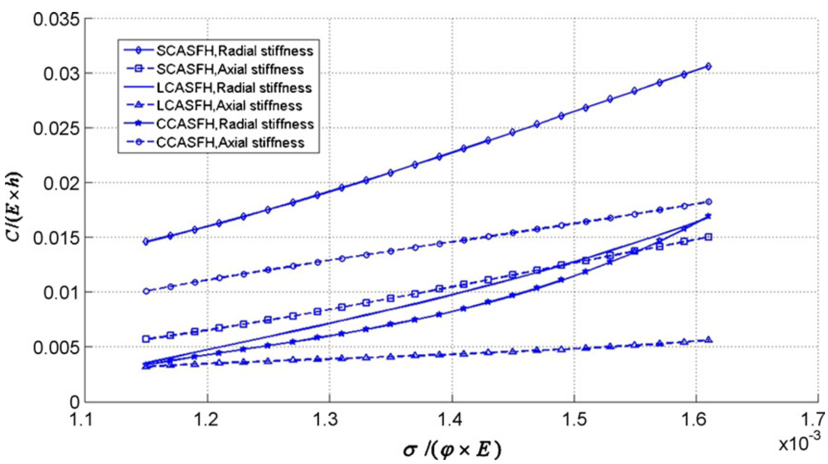

Fig. 13. Comparison stiffness in radial and axial-direction.

comparison is made between the properties of the flexure hinges comparing on the basis of identical function means: equal rotation angle and stress. This is visualized in Figs. 13 and 14. There from several conclusions are drawn:

Defining

$$\gamma = \frac{\sigma}{\varphi \times E} \tag{21}$$

- As shown in Fig. 13, SCASFH has the best radial stiffness and the radial stiffness of CCASFH is worst. CCASFH has the best axial stiffness and the axial stiffness of LCASFH is worst.
- As shown in Fig. 14, SCASFH has the best rotation stiffness. While $\gamma < 1.2$, rotation stiffness of LCASFH is better than CCASFH. While $\gamma > 1.2$, rotation stiffness of CCASFH is better than LCASFH.

6. The application of design graph

In order to introduce the use of dimensionless equations and graphs to design annulus-shaped flexure hinge, three calculation examples are given below:

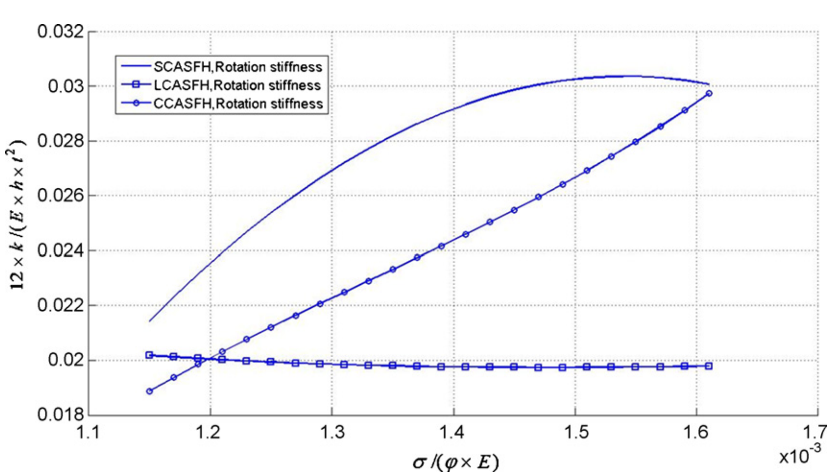

Fig. 14. Comparison rotation stiffness.

Consider a SCASFH which rotates from −3° to +3° (total angle 6°). Using titanium alloy, the allowed stress level is 460 MPa and the Young's modulus is 95 GPa. The dimensionless number for rotation stress now becomes (6 decimal places):

$$\frac{\sigma}{\varphi \times E} = 0.001614 \tag{22}$$

The dimensionless factor for the SCASFH is found from the graph, or Eq. (9) (3 decimal places):

$$\varsigma = 0.135 \tag{23}$$

Supposing the thickness of designed flexure hinges as (2 significant digits):

$$h = 10\ \text{mm} \tag{24}$$

The stiffness in radial and axial-direction, can be derived directly (5 significant digits):

$$C_{\text{radial}} = 29.165 \times 10^6\ \text{N/m} \tag{25}$$

$$C_{\text{axial}} = 14.345 \times 10^6\ \text{N/m} \tag{26}$$

These stiffness values can be compared to the desired situation, as commonly derived from dynamic performance specifications of the mechanism. For a higher stiffness, or better dynamic performance, concessions have to be made regarding the rotation angle, the allowed stress or the plate thickness. If an acceptable stiffness is found, the only remaining parameter is 't'. This value should take into account the manufacturing capability. For example the thickness of SCASFH can be taken (2 significant digits):

$$t = 0.15\ \text{mm} \tag{27}$$

Then the rotational stiffness can now be derived (4 decimal places):

$$k = 0.0536\ \text{Nm/}^{\circ} \tag{28}$$

This value can be used to calculate the torque which the actuator has to deliver. Supposing the lump length of SBFE as (2 significant digits)

$$B = 4.0\ \text{mm} \tag{29}$$

then the length of SBFE is (3 significant digits):

$$L = 8.21\,\text{mm}$$

If the diameter of inner circle of annulus-shaped flexure hinge is not 4 mm, the following transformation has to be made:

$$\theta = 2\ \sin^{-1}\left(\frac{D}{D_0}\sin\frac{\theta}{2}\right) \tag{30}$$

where θ is rotation angle used in the dimensionless equations, θ is demanded rotation angle, D is demanded inner circle diameter, and D_0 is constant which equals 4 mm.

Hence a 3D model can be established based on the structure parameters mentioned above. Finite element analysis result shows that the rotational stroke is between −3.07° and +3.07° (total angle 6.14°) and a relative error is 2.5%.

Consider a LCASFH which rotates from −4° to +4° (total angle 8°). The parameters are given in Table 5.

A 3D model is established based on structure parameters which are mentioned above. Analysis shows results for rotational stroke between −4.12° and +4.12° (total angle 8.24°) and a relative error is 3%.

Consider a CCASFH which rotates from −5° to +5° (total angle 10°). The parameters are given in Table 6.

A 3D model is established based on structure parameters which are mentioned above. Analysis shows results for rotational stroke is between −4.8° and +4.8° (total angle 9.6°) and a relative error is 4%.

Table 5
Parameters of LCASFH.

ζ	0.093
C_{radial}	4.713×10^6 N/m
C_{axial}	3.325×10^6 N/m
t	0.15 mm
k	0.0356 N m/°
h	10 mm
L	23.34 mm
B	5 mm

Table 6
Parameters of CCASFH.

ξ	0.163
C_{radial}	1.59×10^6 N/m
C_{axial}	6.517×10^6 N/m
t	0.15
k	0.0269 N m/°
h	10 mm
P	15 mm
R	40.09 mm

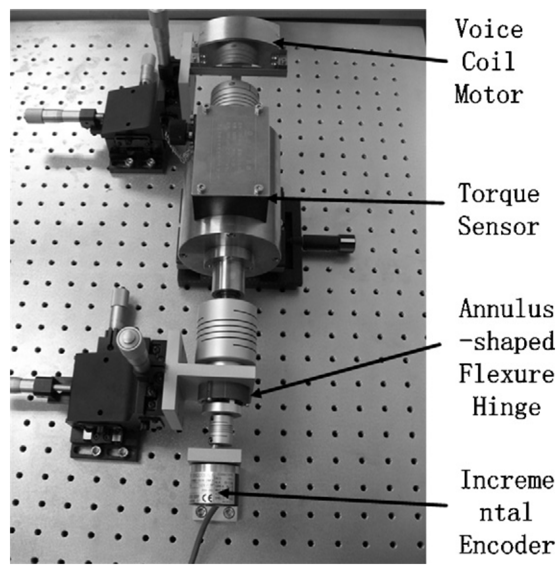

Fig. 15. Test equipment.

Table 7
Test results.

	Design value	Test value
SCASFH	±3°	±3°
LCASFH	±4°	±4.1°
CCASFH	±5°	±5.3°

Three types of annulus-shaped flexure hinges mentioned above are manufactured using slow-feeding NC wire-cut machine (ROBOFIL 380) and manufacture accuracy is 3 μm. The test equipment is shown in Fig. 15. Voice coil motor is used to drive the flexure hinge. Torque sensor measures the rotational torque. Incremental encoder feeds back rotational angle. The test results are given in Table 7.

7. Conclusion

For SCASFH, LCASFH and CCASFH, dimensionless design graphs and equations are constructed by the use of structure-interrelated dimensionless factor. Using these graphs, designers can determine the geometry of annulus-shaped flexure hinge fast based on the demand design.

In this paper, the attention is focused on the stress and stiffness behavior of annulus-shaped flexure hinges. Based on the design graphs, a comparison is drawn between the properties of the flexure hinges, when compared on basis of identical function: equal rotation angle and stress. SCASFH is preferred above LCASFH and CCASFH when radial stiffness or rotation stiffness is absolutely demanded. CCASFH has the best axial stiffness.

Three calculation examples are given to validate the dimensionless design graphs and equations. The results indicate a rotation stroke with a relative error below 4%. Dimensionless design graph method is suitable for designing annulus-shaped flexure hinge.

Acknowledgements

The authors gratefully acknowledge the financial support of the NSFC (Grant No. 50675007) and NCET Program (Grant No. NCET-06-0165) in Universities of China.

References

[1] Bao MH, Sun YC, Zhou J, Huang YP. Squeeze-film air damping of a torsion mirror at a finite tilting angle. Journal of Micromechanics and Microengineering 2006;16:2330–415.

[2] Henein S, Aymon C, Bottinelli S, Clavel R. Articulated structures with flexible joints dedicated to high precision robotics. In: Proceedings of the international advanced robotics programme: workshop on microrobots, micromachines and systems. Russia: IEEE; 1999. p. 135–40.

[3] Jacobsen JO, Howell LL, Magleby SP. Components for the design of lamina emergent mechanisms. In: Proceedings of IMECE. 2007. IMECE2007-42311.

[4] Kim D, Kang D, Shim J, Song I, Gweon D. Optimal design of a flexure hinge-based XYZ atomic force microscopy scanner for minimizing Abbe errors. Review of Scientific Instrument 2005;76:073706.

[5] Hinkley D, Simburger EJ. A multifunctional flexure hinge for deploying omnidirectional solar arrays. In: Proceedings of the 42nd AIAA/ASME/ASCE/AHS/ASC structures, structural dynamics, and materials conference and exhibit. 2001.

[6] CSEM Center Suisse d'Electronique et de Microtechnique SA. Flexure elements. http://www.csem.ch/fs/micro_mechatronics.htm.

[7] Rotary Flexure [P]. US 6146044 (A). November 14; 2000.

[8] Guerinot AE, Magleby SP, Howell LL, Todd RH. Compliant joint design principles for high compressive load situations. Journal of Mechanical Design, Transactions of the ASME 2005;127:774–81.

[9] Lobontiu N, Paine Jeffrey SN, O'Malley E, Samuelson M. Parabolic and hyperbolic flexure hinges: flexibility, motion precision and stress characterization based on compliance closed-form equation. Precision Engineering 2002;26(2):183–92.

[10] Masters ND, Howell LL. A three degree-of-freedom model for self-retracting fully compliant bistable micromechanisms. ASME Journal of Mechanical Design 2005;127:739–44.

[11] Xu D, Ananthasuresh GK. Freeform skeletal shape optimization of compliant mechanisms. ASME Journal of Mechanical Design 2003;125:253–61.

[12] Tai K, Cui GY, Ray T. Design synthesis of path generating compliant mechanisms by evolutionary optimization of topology and shape. ASME Journal of Mechanical Design 2002;124(3):492–500.

[13] Smaili A, Diab N, Atallah N. Optimum synthesis of mechanisms using Tabu-gradient search algorithm. ASME Journal of Mechanical Design 2004;127(5):917–23.

[14] Saxena A, Ananthasuresh GK. On the optimality property of complaint topologies. Structural and Multidisciplinary Optimization 2000;19(1):36–49.

[15] Smith ST. Flexure: elements of elastic mechanisms. Gordon Breach Science 2000.

[16] Xu P, Jingjun Y, Guanghua Z, Shusheng B, Zhiwei Y. Analysis of rotational precision for an isosceles-trapezoidal flexural pivot. ASME Journal of Mechanical Design 2008;130(5):052302.